Spatial Modulation

Raed Y. Mesleh, *Member, IEEE*, Harald Haas, *Member, IEEE*, Sinan Sinanović, Chang Wook Ahn, *Member, IEEE*, and Sangboh Yun, *Member, IEEE*

***Abstract*—Spatial modulation (SM) is a recently developed transmission technique that uses multiple antennas. The basic idea is to map a block of information bits to two information carrying units: 1) a symbol that was chosen from a constellation diagram and 2) a unique transmit antenna number that was chosen from a set of transmit antennas. The use of the transmit antenna number as an information-bearing unit increases the overall spectral efficiency by the base-two logarithm of the number of transmit antennas. At the receiver, a maximum receive ratio combining algorithm is used to retrieve the transmitted block of information bits. Here, we apply SM to orthogonal frequency division multiplexing (OFDM) transmission. We develop an analytical approach for symbol error ratio (SER) analysis of the SM algorithm in independent identically distributed (i.i.d.) Rayleigh channels. The analytical and simulation results closely match. The performance and the receiver complexity of the SM–OFDM technique are compared to those of the vertical Bell Labs layered space–time (V-BLAST–OFDM) and Alamouti–OFDM algorithms. V-BLAST uses minimum mean square error (MMSE) detection with ordered successive interference cancellation. The combined effect of spatial correlation, mutual antenna coupling, and Rician fading on both coded and uncoded systems are presented. It is shown that, for the same spectral efficiency, SM results in a reduction of around 90% in receiver complexity as compared to V-BLAST and nearly the same receiver complexity as Alamouti. In addition, we show that SM achieves better performance in all studied channel conditions, as compared with other techniques. It is also shown to efficiently work for any configuration of transmit and receive antennas, even for the case of fewer receive antennas than transmit antennas.**

***Index Terms*—Interchannel interference (ICI), multiple-input–multiple-output (MIMO), orthogonal frequency division multiplexing (OFDM), receiver complexity, space–time coding (STC) coded modulation, spatial modulation (SM), vertical Bell Labs layered space–time (V-BLAST).**

Manuscript received June 12, 2006; revised February 20, 2007, June 29, 2007, September 4, 2007, and September 18, 2007. This work was supported by the Samsung Advanced Institute of Technology, Suwon, Korea. The review of this paper was coordinated by Prof. E. Bonek.

R. Y. Mesleh is with the School of Electrical Engineering and Computer Science, Jacobs University, D-28759 Bremen, Germany (e-mail: r.mesleh@jacobs-university.de).

H. Haas is with the Institute for Digital Communications, University of Edinburgh, EH9 3JL Edinburgh, U.K., and also with Jacobs University, D-28759 Bremen, Germany (e-mail: h.haas@ed.ac.uk).

S. Sinanović is with the Institute for Digital Communications, University of Edinburgh, EH9 3JL Edinburgh, U.K. (e-mail: s.sinanovic@ed.ac.uk).

C. W. Ahn was with Gwangju Institute of Science and Technology, Gwangju 500-712, Korea. He is now with the Department of Computer Engineering, Sungkyunkwan University, Suwon 440-746, Korea (e-mail: cwan@evolution.re.kr).

S. Yun is with the Telecommunication R&D Center, Samsung Electronics Company, Ltd., Suwon 442-600, Korea (e-mail: sbyun@samsung.com).

Color versions of one or more of the figures in this paper are available online at http://ieeexplore.ieee.org.

Digital Object Identifier 10.1109/TVT.2008.912136

I. Introduction

THE NEED for high data rate and high spectral efficiency are the key elements that drive research in future wireless communication systems [53]. Adaptive coding and modulation, iterative (turbo) decoding algorithms, space–time coding (STC), multiple antennas and multiple-input–multiple-output (MIMO) systems, multicarrier modulation, and ultra wideband radio are examples of enabling technologies for next-generation wireless communication. Among the set of existing technologies, MIMO orthogonal frequency division multiplexing (MIMO–OFDM) with adaptive coding and modulation is a promising candidate for future wireless systems. A MIMO system boosts spectral efficiency by using multiple antennas to simultaneously transmit data to the receiver [1]–[4]. OFDM converts a frequency-selective channel into a parallel collection of frequency flat-fading subchannels, in which the available bandwidth is very efficiently used [5]. The OFDM technique has been adopted in several wireless standards such as digital audio and video broadcasting, the IEEE 802.11a standard [6], the IEEE 802.16a metropolitan area network standard, and the local area network standard [7].

There are three main categories of MIMO techniques. The first category improves power efficiency by maximizing spatial diversity, e.g., using delay diversity [8], [9]. In such systems (e.g., STC), the capacity improvement results from diversity gain, which reduces the bit error probability for the same spectral efficiency. However, the maximum spectral efficiency of full-diversity STC systems is one symbol per symbol duration for any number of transmit antennas [9]. These systems can be designed to achieve full diversity gain with very low receiver complexity. In addition, STCs are well known to combat channel imperfections that exist in real-time implementations of MIMO systems [10], [11]. The second category of MIMO techniques exploits knowledge of the channel at the transmitter. It decomposes the channel matrix by using singular value decomposition and uses the resulting unitary matrices as prefilters and postfilters at the transmitter and receiver, respectively, to achieve capacity gain [12], [13]. In this paper, channel information is assumed to be known only at the receiver, with no channel information at the transmitter. Therefore, these techniques are not implemented here, but possible scenarios will briefly be discussed in future works.

The third type of MIMO technique uses a layered space–time approach to transmit multiple independent data streams over the antennas to increase capacity. A well-known technique is the Bell Labs layered space–time (BLAST) architecture [3]. The BLAST scheme demultiplexes a user data stream into a number of substreams that are equal to the number of transmission antennas. Two types of BLAST realizations have

widely been discussed: 1) diagonal BLAST (D-BLAST) [3] and 2) vertical BLAST (V-BLAST) [14].

The D-BLAST architecture is considered the reference in performance for MIMO systems, since it can reach capacities near the Shannon limit [15]. The D-BLAST system has a diagonal layered STC architecture with sequential nulling and interference cancellation decoding. However, it suffers from boundary wastage at the start and at the end of each packet, and its complexity is very high to be practical [16]. The V-BLAST architecture is a simplified version of D-BLAST, which tries to overcome its limitations. However, in doing so, the transmit diversity is lost. It has been demonstrated that, with the V-BLAST algorithm, spectral efficiencies of 20–40 b/s/Hz can be achieved in an indoor rich scattering propagation environment, assuming a practical signal-to-noise ratio (SNR) range and bit error performance, respectively [14].

Several problems are encountered in the development of multiple antenna transmission schemes [17]–[20]. These problems arise from several sources, among which are the following.

1) BLAST transmission systems suffer from high interchannel interference (ICI) at the receiver due to simultaneous transmissions on the same frequency from multiple antennas.
2) The high ICI requires a complex receiver algorithm, which increases the overall system complexity.
3) System performance is traded off with receiver complexity. In addition, although BLAST systems achieve a relatively good performance in ideal channel conditions, their performance severely degrades under nonideal channel conditions [17], [18].
4) With full-diversity STCs, these limitations are overcome. In addition, due to their orthogonal design, they can easily be decoded at the receiver side. STCs are also robust in the presence of channel imperfections [10], [11]. However, the maximum spectral efficiency of full-diversity STC systems is one symbol per symbol duration for any number of transmit antennas. In other words, for full-diversity STCs to achieve spectral efficiency that is similar to that of BLAST techniques, they need to use higher modulation orders.
5) For efficient operation of BLAST techniques, the number of transmit antennas must be less than or equal to the number of receive antennas [16]. In STCs, the situation is different. Generally, STCs can be designed for different numbers of transmit and receive antennas and can efficiently work, even if the number of receive antennas is less than the number of transmit antennas. However, an orthogonal design of full-rate-code STC is only known for the case of two transmit antennas, and there is no known solution for a higher number of transmit antennas. Therefore, the design of STCs for more than two transmit antennas must sacrifice a portion of the data rate to achieve full orthogonality and, hence, full diversity.

One approach for dealing with these issues is to use *spatial modulation* (*SM*) [21]–[23]. In this case, only one transmit antenna is active at any instant. The active transmit antenna number is an added source of information that is exploited by SM to boost the spectral efficiency. That is why SM is different from other MIMO techniques such as space–time bit-interleaved coded modulation [24], in which the antenna pattern is recognized as a spatial constellation but is not used as a source of information.

In SM, a block of any number of information bits is mapped into a constellation point in the signal domain and a constellation point in the spatial domain. At each time instant, only one transmit antenna of the set will be active. The other antennas will transmit zero power. Therefore, ICI at the receiver and the need to synchronize the transmit antennas are completely avoided. At the receiver, maximum receive ratio combining (MRRC) is used to estimate the transmit antenna number, after which the transmitted symbol is estimated. These two estimates are used by the spatial demodulator to retrieve the block of information bits.

In this paper, a closed-form analytical symbol error ratio (SER) of SM in independent identically distributed (i.i.d.) Rayleigh channels is derived. Analytical and simulation results closely match over a wide range of SNR values. The assumption of i.i.d. channel conditions is idealized, and we chose it to simplify the analytical calculations; it is not a practical model for MIMO–OFDM systems. However, further investigation in this paper includes nonidealistic channel conditions, in which the BER is simulated for SM–OFDM, V-BLAST–OFDM [25], and Alamouti–OFDM [26]. We also compare receiver complexity for these systems. The combined effect of nonidealistic channel conditions, including spatial correlation (SC), mutual antenna coupling (MC), and Rician fading, on both coded and uncoded systems is discussed.

The rest of this paper is organized as follows. Section II presents the SM idea and its application to OFDM transmission. Analytical calculation of SER for SM is, then, shown in Section III, as well as a comparison between the analytical and the simulation results. The channel model and the modeling of Rician fading, SC, and MC channel imperfections are discussed in Section IV. Simulation results and the receiver complexity comparison follow in Sections V and VI, respectively. Finally, Section VII concludes this paper.

II. SM–OFDM System Model

The following notations are used throughout this paper. Bold and lowercase letters denote vectors, whereas bold and capital letters denote matrices. The notations $(\cdot)^+$, $(\cdot)^H$, and $(\cdot)^T$ denote the pseudoinverse, Hermitian, and transpose of a vector or matrix, respectively, and $(\cdot)^{-1}$ denotes the inverse of a matrix.

The SM–OFDM system model is shown in Fig. 1.

$\mathbf{Q}(k)$ is an $\tilde{m} \times n$ binary matrix that will be transmitted in one OFDM symbol, where $\tilde{m}$ is the total number of bits per symbol per subchannel, and n is the total number of OFDM subchannels. The SM maps this matrix into another matrix $\mathbf{X}(k)$ of size $N_t \times n$, where N_t is the total number of transmit antennas, by using the SM mapping table shown in Fig. 1. This table maps each column in $\mathbf{Q}(k)$ into a binary phase-shift keying (BPSK) constellation point and a single transmit antenna number from a set of four antennas. BPSK

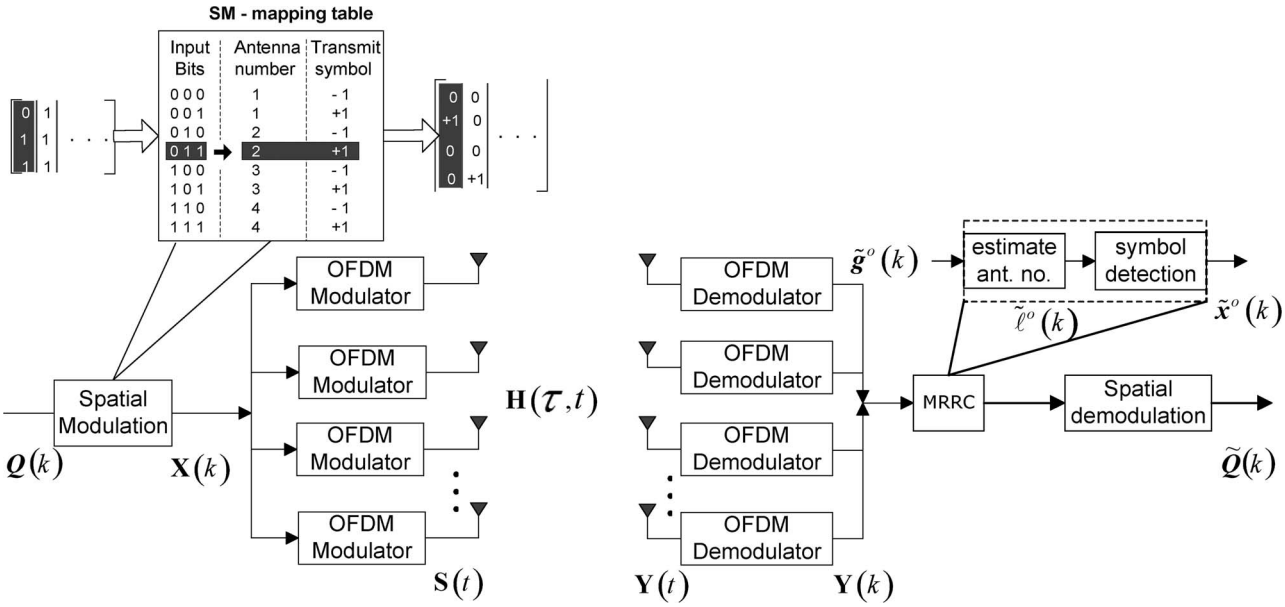

Fig. 1. SM–OFDM system model.

and four transmit antennas are considered as an example here. In general, any number of transmit antennas and any digital modulation scheme can be used. The constellation diagram and the number of transmit antennas determine the total number of bits to be transmitted on each subchannel at each instant. The combination of BPSK and four transmit antennas in this illustration results in a total of three information bits to be transmitted on each subchannel. Instead, four quadrature-amplitude modulation (QAM) and two transmit antennas can be used to transmit the same number of information bits, as shown in Table I. The number of bits that can be transmitted on each OFDM subchannel for a system that uses a QAM constellation diagram of size M $(m = \log_2(M))$ and N_t transmit antennas is [22]

$$\tilde{m} = \log_2(N_t) + m. \tag{1}$$

TABLE I
SM MAPPING TABLE: 3 b/SYMBOL/SUBCHANNEL

Input bits	N_t=2, M=4		N_t=4, M=2	
	Antenna number	Transmit symbol	Antenna number	Transmit symbol
000	1	+1+j	1	-1
001	1	-1+j	1	+1
010	1	-1-j	2	-1
011	1	+1-j	2	+1
100	2	+1+j	3	-1
101	2	-1+j	3	+1
110	2	-1-j	4	-1
111	2	+1-j	4	+1

This shows that the constellation diagram and the number of transmit antennas can be traded off for any number of transmitted information bits. In addition, SM increases the spectral efficiency by the base-two logarithm of the total number of transmit antennas. This can be viewed as a disadvantage for a large number of transmit antennas as compared to, for example, V-BLAST. Note that, in V-BLAST, the spectral efficiency linearly increases with the number of transmit antennas. For example, consider a MIMO system with eight transmit and receive antennas. If V-BLAST is used with 16 QAM, a spectral efficiency of 32 b/s/Hz can be achieved. However, if SM is used with the same configuration and modulation order, the spectral efficiency is only 7 b/s/Hz. In order for SM to achieve the spectral efficiency of V-BLAST with 16 QAM, it requires 2^{28} transmit antennas, which is not feasible. This means that SM cannot compete with V-BLAST when a large number of antennas and high modulation orders are involved. However, it is generally accepted that a large number of transmit antennas is impractical with current technology, particularly when considering the cost that comes from adding antennas for an end-user system. For instance, two competing approaches have been proposed for the MIMO-oriented version of the IEEE 802.11n standard: 1) one with a 2×2 MIMO matrix and 2) another with a 4×4 matrix. The current 802.11n draft provides for up to four transmit antennas, even though compliant hardware is not required to support that many antennas [27].

With SM mapping, the matrix $\mathbf{X}(k)$ has one nonzero element in each column at the position of the mapped transmit antenna number. All other elements in that column are set to zero. For instance, in Fig. 1, an input bit sequence of $[0\ 1\ 1]^T$ [highlighted column vector in $\mathbf{Q}(k)$] is mapped to the BPSK symbol $+1$ and the second transmit antenna by using the SM mapping table. This means that only the second antenna transmits this symbol on the first OFDM subchannel, whereas all other antennas transmit zero power. As a result, the first column vector in $\mathbf{X}(k)$ is $[0 + 1\ 0\ 0]^T$. The second bit sequence is $[1\ 1\ 1]^T$ and is mapped to $[0\ 0\ 0 + 1]^T$, and so on. The resulting symbols in each row vector $\mathbf{x}_\kappa(k)$ are the data that will be transmitted on all subchannels and from antenna κ. Then, each row vector $\mathbf{x}_\kappa(k)$ is modulated using an OFDM modulator.

The resulting output vectors at the OFDM modulator are simultaneously transmitted from the N_t transmit antennas over the MIMO channel $\mathbf{H}(\tau, t)$. At the receiver, the rows of the received matrix $\mathbf{Y}(t) = \mathbf{H}(\tau, t) \otimes \mathbf{S}(t) + \mathbf{R}(t)$, where $\mathbf{S}(t)$ is a matrix that contains all OFDM symbols that are transmitted from all transmit antennas, $\mathbf{R}(t)$ is the additive white Gaussian noise (AWGN) matrix, and $\otimes$ denotes time convolution, are demodulated using N_r OFDM demodulators. In the following, discrete time representation is considered. The output from the OFDM demodulators is a matrix $\mathbf{Y}(k)$ of size $N_r \times n$, each column of which corresponds to the received data in the n OFDM subchannels from the N_r receive antennas.

In the following, MRRC is used to detect the transmit antenna number and the transmitted symbol in the frequency domain for each OFDM subchannel. The following notations are for a single OFDM subchannel, and the generalization to multiple subchannels is straightforward by simply adding an additional subscript. However, for reasons of clarity, this is left out. The MRRC algorithm multiplies the Hermitian conjugate of the frequency response channel matrix for each subchannel, which is assumed to be known at the receiver, with the received column vector at this particular subchannel, i.e.,

$$\mathbf{g}(k) = \mathbf{H}^H(k)\mathbf{y}(k) \tag{2}$$

where $\mathbf{H}$ is the $N_r \times N_t$ discrete time-invariant frequency response channel matrix, and $\mathbf{y}$ is the corresponding demodulated OFDM vector of length N_r. In an ideal scenario, where there is perfect time and frequency synchronization and no noise, $\mathbf{g}(k)$ is the same as $\mathbf{x}(k)$, since by definition, $\mathbf{x}(k)$ contains only one element that is different from zero. Therefore, in the presence of AWGN, the estimated transmit antenna number $\tilde{\ell}$ at time instant k is the index or position of that element in $\mathbf{g}(k)$, whose absolute value is maximum, i.e.,

$$\tilde{\ell} = \arg\max_{\forall i} \left(|g_i(k)|\right) \qquad i = 1, \ldots, N_t. \tag{3}$$

Assuming that the estimate of the transmit antenna number is correct, the transmitted symbol at this instant can be estimated as follows:

$$\tilde{x}(k) = Q\left[g_{i=\tilde{\ell}}(k)\right] \tag{4}$$

where $g_{i=\tilde{\ell}}$ is the element number $\tilde{\ell}$ in the column vector $\mathbf{g}(k)$, and $Q(\cdot)$ is the constellation quantization (slicing) function.

These two estimates are, then, used by the SM demodulator to retrieve the transmitted information bits on this particular subchannel by an inverse mapping process that uses the same mapping table that was used at the transmitter.

III. Analytical SER Calculation of SM

Computation of the analytical performance of SM is not straightforward. There are two estimation processes that are involved: 1) The transmit antenna number is estimated, and 2) the transmitted symbol is estimated. The two processes are assumed to be independent in the calculation. However, this is not generally correct. For instance, if the channel paths are correlated, the two estimation processes will be dependent, and the following derived equation is the upper bound on the true performance in such channel conditions. The bits are correctly recovered only if both estimates are correct. To compute the overall probability of error P_e, let P_a denote the probability that the estimate of the antenna number is incorrect, and let P_d be the probability that the transmitted symbol estimate is incorrect. Then, the retrieved SM bits are correct if and only if the estimates of the antenna number and the transmitted symbol are both correct. The probability of that is

$$P_c = (1 - P_a)(1 - P_d). \tag{5}$$

The probability that the demapped bits are incorrect is, then, $1 - P_c$ and can be written as

$$P_e = P_a + P_d - P_d P_a. \tag{6}$$

If there is only one transmit antenna, then P_a is zero, and the overall probability of error is reduced to the case of MRRC with multiple receive antennas, which is an upper bound for SM performance. However, the use of multiple transmit antennas in SM results in an increase in the overall probability of error. This increase in P_e is evident by noting that $1 \geq (P_a \text{ and } P_d) \geq 0$. Hence, SM increases the SER by $P_a - P_d\, P_a \geq 0$ as compared to MRRC.

In Sections III-A–C, the SER of each estimation process is considered separately.

A. Analytical SER of the Transmitted Symbol Estimation Process

As discussed in Section III, the estimation of the transmitted symbol for any M-QAM is a $1 \times N_r$ MRRC detection, since only the corresponding element in the resulting vector is considered for the estimation process. The average SER of a square M-QAM over generalized fading channels is [28]

$$P_d = \frac{4}{\pi}\left(1 - \frac{1}{\sqrt{M}}\right)\int_0^{\frac{\pi}{2}} \prod_{l=1}^{N_r} \mathcal{M}_{il}\left(\frac{-g_{QAM}}{\sin^2(\phi)}; \bar{\gamma}_l\right) d\phi$$
$$-\frac{4}{\pi}\left(1 - \frac{1}{\sqrt{M}}\right)^2 \int_0^{\frac{\pi}{4}} \prod_{l=1}^{N_r} \mathcal{M}_{il}\left(\frac{-g_{QAM}}{\sin^2(\phi)}; \bar{\gamma}_l\right) d\phi \tag{7}$$

where

$$g_{QAM} = \frac{3}{2(M-1)},$$
$$M_{il}\left(\frac{-g_{QAM}}{\sin^2(\phi)}; \bar{\gamma} l\right) = \left(1 + \frac{g_{QAM}\bar{\gamma} l}{\sin^2(\phi)}\right)^{-1}$$

is the moment-generating function for Rayleigh flat-fading channels, and $\bar{\gamma}_l$ is the average SNR at each receive antenna.

B. Analytical Error Calculation of the Transmit Antenna Number Estimation Process

In the following, the computation of P_a is considered. For simplicity, only four transmit antennas are considered for the

derivation, and the result is later generalized to any number of transmit antennas.

The antenna number estimate is the position of the maximum absolute value of all elements in the vector that results from MRRC. This corresponds to finding the element with the greatest magnitude in the spatial domain among a set of N_t elements.

At a specific time instant and for a 4×4 transmission scenario, let $\mathbf{H} = [\mathbf{h}_1, \mathbf{h}_2, \mathbf{h}_3, \mathbf{h}_4]$ be the channel matrix, and let $\mathbf{h}_i = [h_{1i}, h_{2i}, h_{3i}, h_{4i}]^T$ be the corresponding channel vector from each transmit antenna to all receive antennas. To illustrate, assume that a sequence of data bits is mapped to symbol s_2 from a square QAM constellation and to the second transmit antenna. Then, the received vector $\mathbf{y} = \mathbf{h}_2 s_2 + \mathbf{n}$ appears at the input of the receive antennas. Applying MRRC to the received vector $\mathbf{y}$, as in (2), results in the following vector:

$$\mathbf{g} = \begin{pmatrix} \mathbf{h}_1^H \mathbf{h}_2 s_2 + \mathbf{h}_1^H \mathbf{n} \\ \mathbf{h}_2^H \mathbf{h}_2 s_2 + \mathbf{h}_2^H \mathbf{n} \\ \mathbf{h}_3^H \mathbf{h}_2 s_2 + \mathbf{h}_3^H \mathbf{n} \\ \mathbf{h}_4^H \mathbf{h}_2 s_2 + \mathbf{h}_4^H \mathbf{n} \end{pmatrix}. \tag{8}$$

Under the assumption of unity channel gains and for i.i.d channels, we have

$$E\left\{\mathbf{h}_i^H \mathbf{h}_k\right\} = \delta_{i,k}, \qquad \delta_{i,k} = \begin{cases} 1, & \text{if } i = k \\ 0, & \text{otherwise.} \end{cases} \tag{9}$$

Therefore, if the noise is assumed to be AWGN with zero mean and σ_n^2 variance, then three elements in the vector $\mathbf{g}$ have zero mean and σ_n^2 variance. The other element, i.e., the second element in (8), has mean s_2 and variance σ_n^2. The square QAM signal can be decomposed into two independent but identical amplitude modulated signals: 1) in phase I and 2) quadrature Q. In what follows, only the real positive part of the QAM constellation is considered for the calculation. Assume that μ_i is the absolute value of the real part of the transmitted symbol s_2. Then, $\boldsymbol{\mu}$ is a vector of length $c = 2^{(m/2)-1}$, which contains the positive real-part elements of the constellation diagram. Let $P(\mu_i)$ denote the probability that the antenna number estimate is incorrect when transmitting μ_i. Then, the average overall probability of error for the antenna number estimate, when considering the real part P_{ar}, is given by

$$P_{\text{ar}} = \frac{1}{c} \sum_{i=1}^{c} P(\mu_i). \tag{10}$$

The imaginary part is identical to the real part and can be calculated in a similar way. The probability that the detection is correct for both real and imaginary parts is the product of two probabilities, namely, $(1 - P_{\text{ar}})(1 - P_{\text{ar}})$. As a result, the overall probability of error, when considering both real and imaginary parts, is given by [29]

$$P_a = 1 - (1 - P_{\text{ar}})^2 = 2P_{\text{ar}} - P_{\text{ar}}^2. \tag{11}$$

The detection of the transmit antenna number is given in (3). Let $x = |v|$, where v is a random variable that follows a Gaussian distribution with mean μ_i and variance σ_n^2. Then, the probability density functions (pdfs) for v and x for each μ_i are

$$f_V\left(v|\mu_i, \sigma_n^2\right) = \frac{1}{\sigma_n \sqrt{2\pi}} \exp^{-\frac{(v-\mu_i)^2}{2\sigma_n^2}}$$

$$f_X\left(x|\mu_i, \sigma_n^2\right) = \frac{1}{\sigma_n \sqrt{2\pi}} \left(\exp^{-\frac{(x-\mu_i)^2}{2\sigma_n^2}} + \exp^{-\frac{(x+\mu_i)^2}{2\sigma_n^2}} \right). \tag{12}$$

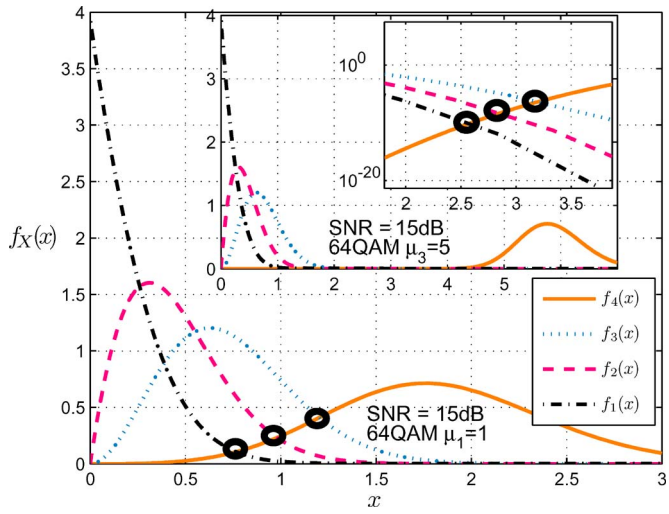

Fig. 2. Order statistics pdfs of four random variables. The main figure shows the pdfs at SNR $= 15$ dB for 64 QAM and for $\mu_1 = 1$, whereas the upper main-corner figure shows the same pdfs at the same SNR but with $\mu_3 = 5$. The small figure inside the corner figure shows the crossing point between the pdfs by plotting the y-axis on log scale. The bold circles in the main figure are the three intersection points of the pdfs. It is clearly shown that the error contribution from the second maximum is the largest, then from the third maximum, and so on.

The second step in estimating the antenna number is finding the position of the element in $\mathbf{g}$ with a maximum absolute value. This is done by computing the pdfs of the sorted N_t random variables, where each has a pdf as given in (12) but with different means. This problem can be treated with order statistics [30].

Let $X_{(1)}, \ldots, X_{(N_t)}$ denote the order statistics of random samples from a continuous population with a cumulative distribution function $F_X(x|\mu_i, \sigma_n^2)$ and a pdf $f_X(x|\mu_i, \sigma_n^2)$, where $X_{(N_t)} > X_{(N_t-1)} > \cdots > X_{(1)}$. Then, the pdf of $X_{(j)}$ is

$$f_{X_{(j)}}\left(x|\mu_i, \sigma_n^2\right) = \frac{n!}{(j-1)!(N_t - j)!} f_X\left(x|\mu_i, \sigma_n^2\right) \times \left[F_X\left(x|\mu_i, \sigma_n^2\right)\right]^{j-1} \times \left[1 - F_X\left(x|\mu_i, \sigma_n^2\right)\right]^{N_t - j}. \tag{13}$$

Considering the current case of four transmit antennas, Fig. 2 shows the order statistics pdfs of the four random variables, which result from taking the maximum of the absolute value of each element in the vector, which results from MRRC at the receiver. If the order statistics pdfs are assumed to be statistically independent, the probability that the antenna number estimation is incorrect can be found by numerically integrating the

intersection areas of $f_{X_{(4)}}(x|\mu_i,\sigma_n^2)$ with all other distributions for each mean value. However, the assumption of statistical independence is an approximate, since the pdfs are derived based on the conditional probability that $X_{(N_t)} > X_{(N_t-1)} > \cdots > X_{(1)}$. Nevertheless, it will be shown in Section III-C that both analytical and simulation results demonstrate a very close match, which indicates that the previous approximations are valid.

Let x_3, x_2, and x_1 indicate the intersection points (bold circles in Fig. 2) between $f_{X_{(4)}}(x|\mu_i,\sigma_n^2)$ and $f_{X_{(3)}}(x|0,\sigma_n^2)$, $f_{X_{(2)}}(x|0,\sigma_n^2)$, and $f_{X_{(1)}}(x|0,\sigma_n^2)$, respectively. Fig. 2 shows that $x_3 > x_2 > x_1 > 0$, which indicates that the error contribution from the second largest sample is always the highest, followed by that of the third largest sample, and so on. The probability of error for each μ_i is, then, given by averaging the multiple hypothesis errors as follows:

$$P(\mu_i) = \frac{1}{3}\left(\int_0^{x_3} f_{X_{(4)}}\left(x|\mu_i,\sigma_n^2\right)dx + \int_0^{x_2} f_{X_{(4)}}\left(x|\mu_i,\sigma_n^2\right)dx + \int_0^{x_1} f_{X_{(4)}}\left(x|\mu_i,\sigma_n^2\right)dx\right). \quad (14)$$

For any number of transmit antennas, (14) can be written as

$$P(\mu_i) = \frac{1}{N_t-1}\left(\sum_{i=1}^{N_{t-1}}\int_0^{x_i} f_{X_{(N_t)}}\left(x|\mu_i,\sigma_n^2\right)dx\right). \quad (15)$$

Knowing $P(\mu_i)$ for $\forall i$, P_{ar} is calculated as in (10). P_{ar} is, then, used to compute P_a as in (11). Both P_a and P_d are used to calculate the overall probability of error as in (6).

C. Analytical and Simulation Results

We next consider the simulation and analytical SER of SM over i.i.d. Rayleigh flat-fading channels for different SM system configurations. The results for a 16-QAM 4×4 SM (resulting in $\tilde{m} = 6$ bits) and a 64-QAM 4×4 SM (resulting in $\tilde{m} = 8$ bits) are depicted in Fig. 3. Additional simulation and analytical results for a 16-QAM 4×3 SM (resulting in $\tilde{m} = 6$ bits) are depicted in Fig. 5.

The simulation and analytical results, as shown in Fig. 3, are in close agreement. At relatively high SNR values, it is not possible to compute the numerical integration, since the crossing points no longer exist, as in, for example, Fig. 4. For a higher modulation order, the crossing points disappear at a higher SNR.

An efficient and practical MIMO architecture must handle any configuration of transmit and receive antennas, including the case of fewer receive antennas than transmit antennas. This is, indeed, required in most cellular systems, since the base station can usually accommodate more transmit antennas than mobile transceivers. The BLAST techniques efficiently work for $N_t \leq N_r$. These techniques result in a poor performance if $N_t = N_r$ and have an error floor if $N_t > N_r$ [31]. Turbo-BLAST is based on a random layered space–time code and an

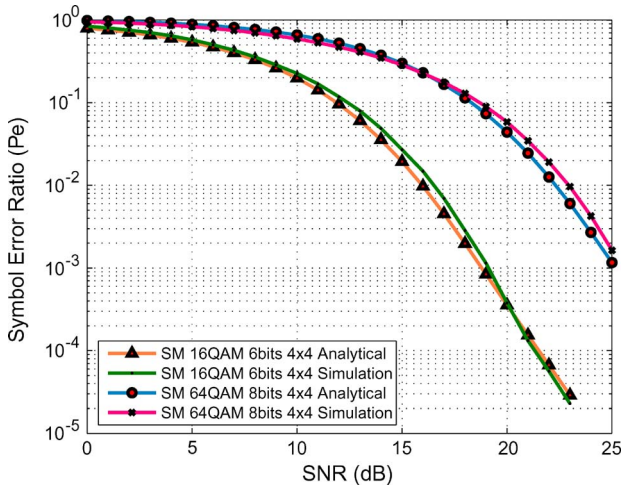

Fig. 3. SMs of 16- and 64-QAM 4×4 analytical and simulation SER.

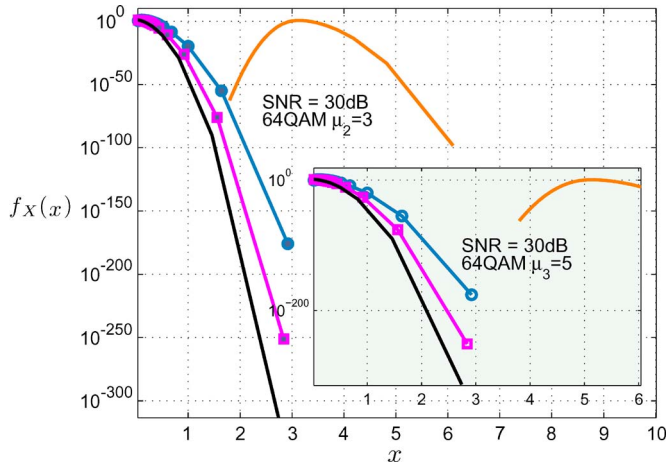

Fig. 4. Order statistics pdfs of four random variables. The main figure shows the pdfs at SNR $= 30$ dB for 64 QAM and for $\mu_2 = 3$, whereas the other figure (figure inside the box) shows the same pdfs at the same SNR but with $\mu_3 = 5$. The figures clearly show that numerical integration is not possible at this high SNR, since the crossing points between the pdfs no longer exist.

iterative detection and decoding receiver. Turbo-BLAST works with any configuration of transmit and receive antennas and has a better performance than traditional BLAST techniques. This, however, comes at the expense of an immense increase in the overall system complexity. An alternative solution is to use SM, as shown in Fig. 5. The results in Fig. 5 show the special case where there are more transmit antennas than receive antennas. The analytical calculation is still valid, and the analytical and simulation results are almost the same.

IV. Channel Models

The multipath frequency selective and time-variant channel model, as well as the Rician fading, SC, and MC channel models, are presented in this section. These models are only relevant to the simulations and the critical assessment of SM as presented in Section V, but they are clearly not a necessary requirement for SM to work.

The channel matrix $\mathbf{H}(\tau,t)$ is a block matrix and can be viewed as a collection of $N_r \times N_t$ vectors of length p, where

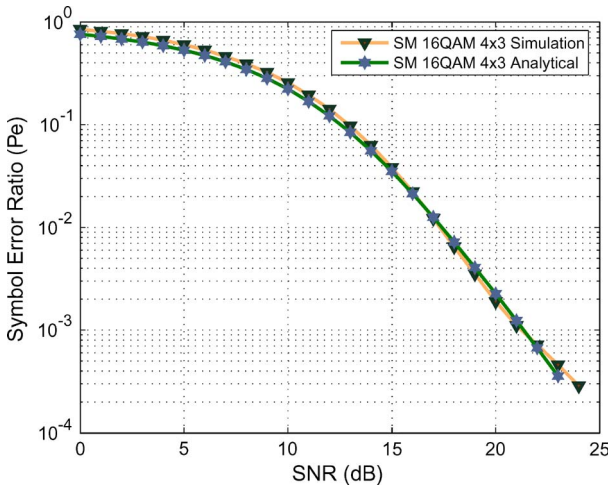

Fig. 5. SM of 16 QAM 4 × 3 analytical and simulation SER.

p is the number of channel paths for each channel link between each transmit antenna and receive antenna. Each vector gives the multipath channel gains between each transmit antenna and receive antenna as follows:

$$\mathbf{H}(\tau,t)=\begin{pmatrix}\mathbf{h}_{1,1}(\tau,t) & \mathbf{h}_{1,2}(\tau,t) & \cdots & \mathbf{h}_{1,N_t}(\tau,t)\\ \mathbf{h}_{2,1}(\tau,t) & \mathbf{h}_{2,2}(\tau,t) & \cdots & \mathbf{h}_{2,N_t}(\tau,t)\\ \vdots & \vdots & \ddots & \vdots\\ \mathbf{h}_{N_r,1}(\tau,t) & \mathbf{h}_{N_r,2}(\tau,t) & \cdots & \mathbf{h}_{N_r,N_t}(\tau,t)\end{pmatrix}. \tag{16}$$

Here, $\mathbf{h}_{\nu,\kappa}(\tau,t)$ is a channel vector of size $p\times 1$ between receive antenna ν and transmit antenna κ, which contains all the multipath channel gains and can be written as

$$\mathbf{h}_{\nu,\kappa}(\tau,t)=\left[h^1_{\nu,\kappa}(\tau_1,t)\, h^2_{\nu,\kappa}(\tau_2,t),\ldots,\, h^p_{\nu,\kappa}(\tau_p,t)\right]^T. \tag{17}$$

In this paper, the multipath channels between different links are taken to be statistically independent and are modeled by the Monte Carlo method [32], [33]. An indoor multipath channel is considered. Each channel path gain is given by

$$h^{\varphi}_{\nu,\kappa}(\tau,t)=\frac{1}{\sqrt{N_h}}\rho[\varphi]\sum_{q=1}^{N_h}e^{j(2\pi f_{\varphi,q}t+\theta_{\varphi,q})}\delta(\tau-\tau_\varphi) \tag{18}$$

where $f_{\varphi,q}=f_d\sin(2\pi u_{\varphi,q})$, $\theta_{\varphi,q}$, and N_h are the discrete Doppler frequencies, the Doppler phases, and the number of harmonic functions, respectively. The propagation delay that is related to the φth channel path is τ_φ. The quantities $u_{\varphi,q}$ are independent random variables, with each having a uniform distribution in the range (0, 1] for all $\varphi=1,2,\cdots,p$ and are independently generated for each link. The maximum Doppler frequency of the frequency selective multipath channel is given by f_d. Finally, the coefficients of the discrete multipath profile are modeled by $\rho[\varphi]$[1] [34].

[1]The channel profile that was used in this paper is $\rho=[1, 0.8487, 0.7663, 0.788, 0.66578, 0.5643, 0.5174, 0.0543, 0.04652]$.

A. Rician Fading Channel

The standard statistical model for a multipath fading channel with a line-of-sight (LOS) component follows a Rician distribution or embodies Rician fading. In Rician fading, the channel impulse response between each transmit antenna κ and receive antenna ν is modeled as the sum of a fixed component and a random multipath channel component [35], which is given by

$$\hat{\mathbf{h}}_{\nu,\kappa}(\tau,t)=\sqrt{\frac{K}{1+K}}\mathbf{h}^{\mathrm{LOS}}_{\nu,\kappa}(\tau,t)+\sqrt{\frac{1}{1+K}}\mathbf{h}_{\nu,\kappa}(\tau,t) \tag{19}$$

where $\mathbf{h}^{\mathrm{LOS}}_{\nu,\kappa}=[1\,0\ldots 0]$ is a $1\times p$ vector, with all components, except for the first one, being set to zero for all ν and κ. $K/(1+K)$ is the mean power of the LOS component, and $1/(1+K)$ is the mean power of the random component. K is defined as the Rician factor.

B. SC Model (Kronecker Model)

The channel correlation depends on both the environment and the spacing of the antenna elements. A terminal, which is surrounded by a large number of local scatterers, can achieve relatively low correlation values, even if the antennas are separated by only half the wavelength. In outdoor base stations, the antennas are significantly higher than the scatterers, and a sufficiently low correlation is likely to require ten wavelengths between neighboring antenna elements. In indoor base stations, the required antenna separation is likely to be between these two extremes [36].

To incorporate the SC into the channel model, the correlation among channels at multiple elements needs to be calculated. The correlated channel matrix is, then, modeled using the Kronecker model for its straightforward mathematical description [37]. It is recognized that this model does not capture all possible correlation scenarios to their full extent [38], but since the interest is a comparative study of different spatial multiplexing techniques, its use is deemed justified. Thus

$$\mathbf{H}^{\mathrm{corr}}(\tau,t)=\mathbf{R}^{1/2}_{\mathrm{rx}}\mathbf{H}(\tau,t)\mathbf{R}^{1/2}_{\mathrm{tx}}. \tag{20}$$

The correlation matrices can be generated using the spatial channel model [39] or can analytically be computed based on the power azimuth spectrum (PAS) distribution and array geometry [37]. In this paper, the latter approach is used, assuming uniform linear arrays with isotropic antenna elements at the transmitter and receiver. In addition, a clustered channel model is assumed, as shown in Fig. 6, in which groups of scatterers are modeled as clusters that are located around the transmit and receive antennas. The calculation of the correlation matrices at the transmitter and the receiver follows the procedure discussed in [37], which is derived based on the PAS distribution and the array geometry. The PAS is modeled as a truncated Laplacian distribution over $(-\pi,\pi]$, since it best fits the measurement results in urban and rural areas [40].

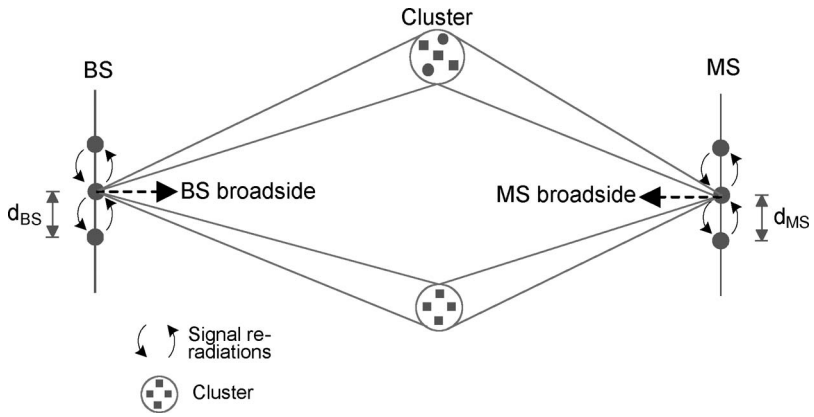

Fig. 6. Geometry of the cluster channel model—SC between transmit/receive signals and MC due to signal reradiations.

C. MC Model

A radio signal that impinges upon an antenna element induces a current in that element, which, in turn, radiates a field that generates a surface current on the surrounding antenna elements. This effect is known as MC. Such a coupling influences the radiation pattern and the antenna correlation. The parameters that affect MC are element separation, frequency, and array geometry [20].

The modified MIMO channel, in the presence of MC at delay time τ, is given by [20]

$$\mathbf{H}^{\text{coup}}(\tau,t)=\frac{\mathbf{Z}_r\mathbf{H}(\tau,t)\mathbf{Z}_t}{c_r c_t}=\mathbf{C}_{\text{rxr}}\mathbf{H}(\tau,t)\mathbf{C}_{\text{txr}} \qquad (21)$$

where $\mathbf{C}_{\text{rxr}}=\mathbf{Z}_r/c_r$ and $\mathbf{C}_{\text{txr}}=\mathbf{Z}_t/c_t$ are receiver and transmitter coupling matrices, and $\mathbf{Z}_r$ and $\mathbf{Z}_t$ are the overall impedance matrices that are shown at the receiver and the transmitter, respectively. c_t and c_r are normalization factors that guarantee that the input and output voltages are the same for zero MC. The impedance matrix for an N-element array with dipole antenna length d_l and dipole radius d_r is calculated as in [20] and [41].

V. Simulation Results

In the simulation, a carrier frequency of 2 GHz with a 20-MHz system bandwidth and 256 OFDM subchannels is assumed. A time-variant multipath channel with a 0.45-μs maximum propagation delay, a 5-Hz Doppler frequency, a 0.5-μs guard interval, and 20 OFDM symbols per frame is considered. The multipath channels of different links are statistically independent. The total signal power is the same for all transmissions. The noise is additive Gaussian, which is spatially and temporally white. Perfect time and frequency synchronization is assumed.

The V-BLAST system uses minimum mean square error (MMSE) detection with ordered successive interference cancellation decoding and assumes knowledge of the SNR at the receiver. The substream with the strongest SNR is first detected, followed by demodulation and subtraction from the initial signal. The detected substream is nulled, and the process is iteratively repeated for all other substreams. In addition, the V-BLAST detection for OFDM is the same as the V-BLAST detection that was used for flat Rayleigh flat-fading channels and can be applied on each subchannel [25]. The Alamouti detection for OFDM follows the same principle as in [8] and [26]. For the Alamouti simulation, a quasistatic channel is assumed, which remains constant for an Alamouti codeword period and is equal to the Alamouti codeword length.

TABLE II
Simulation Configurations. Transmissions of 6 and 8 b/s/Hz, Using SM, V-BLAST, and Alamouti, Are Considered for Simulation

Simulation Configurations			
Transmitted bits	SM	ZF-VBLAST	Alamouti
6 b/s/Hz	4x4 16QAM 2x4 32QAM	3x4 4QAM 2x4 8QAM	2x4 64QAM
8 b/s/Hz	8x4 32QAM 4x4 64QAM	2x4 16QAM	2x4 256QAM

In the following, the bit error rate (BER) performance of coded and uncoded SM–OFDM, Alamouti–OFDM, and V-BLAST–OFDM systems are compared under ideal channel conditions and the combination effects of Rician fading, SC, and MC. In the simulation, all compared systems are selected such that they achieve the same spectral efficiency, as shown in Table II. Two spectral efficiencies are of interest: 1) 6 bits/s/Hz, and 2) 8 bits/s/Hz.

A. Ideal Channel (No Channel Imperfection)

Figs. 7 and 8 show the simulation results under ideal channel conditions for 6- and 8-b/s/Hz transmissions, respectively.

For both fixed spectral efficiencies, all schemes show approximately similar performance at a low SNR (SNR $<$ 10 dB). For SM transmission, the 4×4 system with a 6-b/s/Hz-transmission and the 8×4 system with an 8-b/s/Hz transmission start to show significantly better performance than V-BLAST at SNR $>$ 10 dB, whereas the other SM systems (i.e., the 2×4 system with a 6-b/s/Hz transmission and the 4×4 system with an 8-b/s/Hz transmission) in both figures show better performance gains than V-BLAST at SNR $>$ 20 dB. This can be explained due to the use of a lower modulation order in the first set of systems as compared to the other set. This also explains the behavior of the Alamouti scheme, where Alamouti shows poor performance as compared

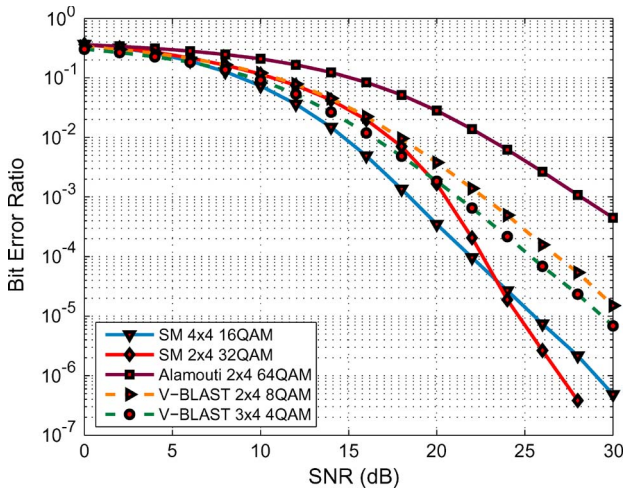

Fig. 7. BER versus SNR for the case of a 6-b/s/Hz transmission (ideal channel).

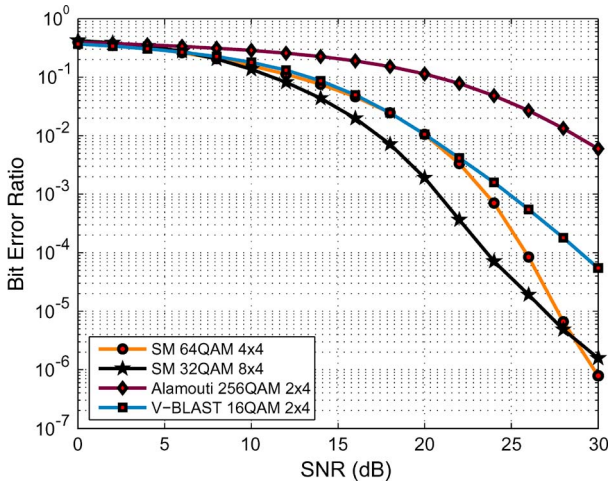

Fig. 8. BER versus SNR for the case of an 8-b/s/Hz transmission (ideal channel).

to SM and V-BLAST. The main reason behind this degradation in Alamouti's performance is the use of a higher constellation size to achieve the same spectral efficiency as in SM and V-BLAST. The performance of SM in both Figs. 7 and 8 demonstrates a major enhancement over V-BLAST and the Alamouti scheme. For example, at a BER of 10^{-3} and for a 6-b/s/Hz transmission, SM outperforms V-BLAST by around 3 dB in the best case and also outperforms Alamouti by around 10 dB. At the same BER and for an 8-b/s/Hz transmission, 8×4 and 4×4 SM systems outperform V-BLAST by around 4 dB and 1 dB, respectively. The Alamouti scheme demonstrates poor performance for the 8-b/s/Hz transmission, and the BER was still greater than 10^{-3}, even at SNR $= 30$ dB. The particular behavior of SM systems is further analyzed, and the results are presented in Fig. 9.

In Fig. 9, the BER performance of SM and MRRC, under similar modulation orders and the same number of receiving antennas, is depicted. At a relatively low SNR, the performance of SM systems approaches that of the corresponding MRRC,

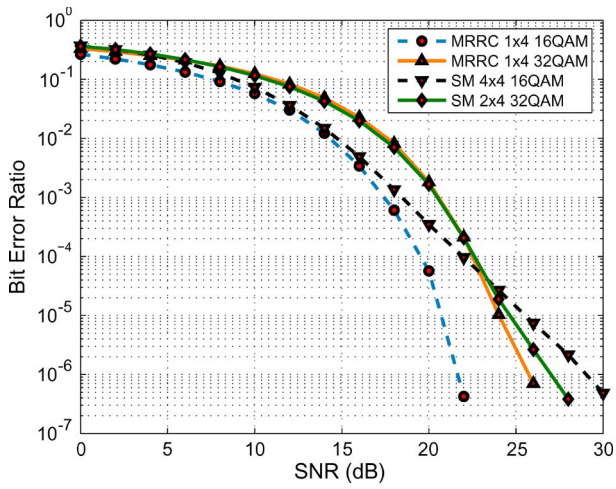

Fig. 9. In SM systems, signal modulation and SM can be traded off to achieve better performance. The figure shows that antenna error dominates for large SNR values, and hence, the 4×4 SM system performs worse than the 2×4 SM system.

which is the upper bound, as discussed in Section III. However, at a higher SNR, the performance of SM systems starts to be poorer than that of MRRC. The 4×4 SM system starts to deviate from MRRC at an SNR of about 16 dB, and at a BER of 10^{-5}, it loses around 5 dB SNR, as compared to MRRC. However, the 2×4 SM system demonstrates better behavior and achieves almost the same performance as MRRC up to an SNR of 23 dB. However, the performance slightly degrades at SNR $>$ 23 dB. This behavior can be explained by the existence of two estimation processes in SM: 1) the antenna number and 2) the transmitted symbol. For a low SNR, the error is dominated by the estimation of the transmitted symbol. For a high SNR, however, the error is dominated by the estimation of the antenna number. Therefore, the likelihood of erroneous antenna detection increases with an increasing number of transmit antennas. Hence, the 2×4 SM system performs better than the 4×4 SM system at a high SNR. This also explains the crossing points of the BER curves of the SM systems in both Figs. 7 and 8.

This is a significant finding, which opens a new area of adaptive modulation, in which the number of transmit antennas and the size of the constellation diagram can be traded off to achieve better performance. For instance, if the channel is bad (resulting in a low SNR at the receiver) and the antennas are almost uncorrelated, it is better to use a smaller signal constellation size and more transmit antennas. On the other hand, if the channel is good, then fewer antennas and a larger signal constellation size achieve better performance.

B. *Uncoded System With All Imperfections*

The effect of all channel imperfections on the performance of SM–OFDM, Alamouti–OFDM, and V-BLAST–OFDM is studied in the following. The Rice factor K in (19) is set to 2 in the presence of LOS. In an indoor environment, the measured values of K are close to the selected value in this paper [42]. SC is present in all systems and at both the transmitter and

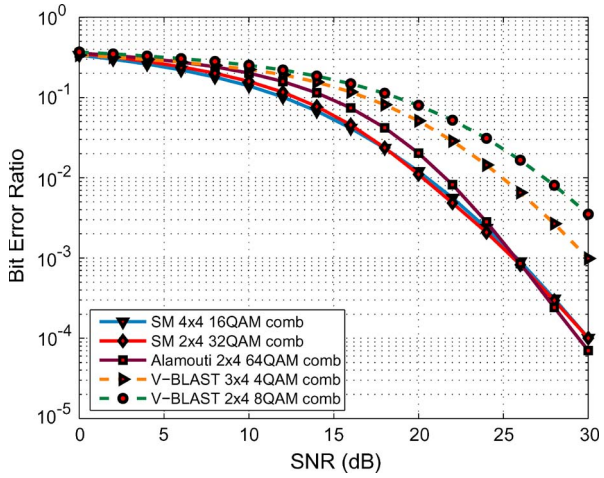

Fig. 10. BER versus SNR for the case of a 6-b/s/Hz transmission (combined channel imperfections).

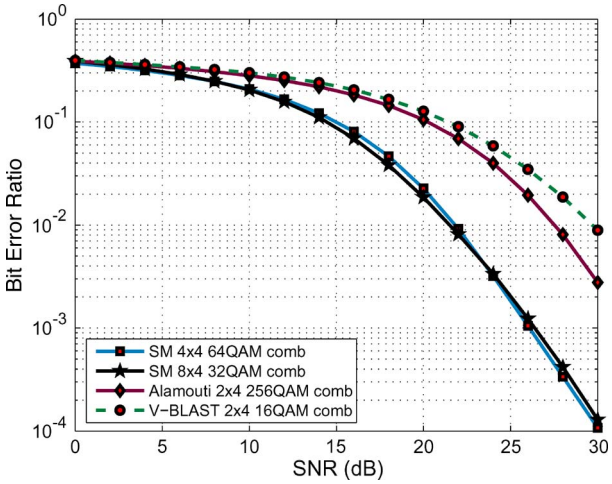

Fig. 11. BER versus SNR for the case of an 8-b/s/Hz transmission (combined channel imperfections).

the receiver arrays. Antenna spacing and the angular values for the simulation of SC are taken from the Third-Generation Partnership Project (3GPP) spatial channel model [39]. The transmit array with an element spacing of 0.5λ, mean angle of arrival of 20°, and an angular spread (AS) of 35° is assumed. The receive array has an element spacing of 10λ, a mean angle of departure of 20°, and an AS of 5°. The MC effect is negligible for an antenna spacing that is beyond λ. Therefore, MC is only present at the transmitter in all systems. To simulate the MC matrix, a uniform linear array with identical dipole antenna elements with an isotropic radiation pattern is assumed. A dipole antenna length of 0.5λ and a radius of $3.33 \times 10^{-3}\lambda$ are considered.

The effect of all channel imperfections on the performance of SM, V-BLAST, and Alamouti is depicted in Figs. 10 and 11 for 6- and 8-b/s/Hz transmissions, respectively.

Combined imperfections degrade the performance of SM and V-BLAST, whereas it enhances Alamouti's performance. The enhancement in Alamouti's performance, as compared to the ideal case, comes from the presence of the LOS component and depends on the constellation size that was used, as well as the value of the Rician factor K [10], [11], [43]. The first important observation is that, for the 6-b/s/Hz transmission (Fig. 10), Alamouti performs slightly worse than SM at a low SNR but has an almost-similar performance at a high SNR. In addition, due to full diversity gains, Alamouti is robust to the presence of SC and MC imperfections [44], [45]. Furthermore, SM performs 1 dB better than Alamouti for SNR $<$ 25 dB. The gain of SM over Alamouti for the 8-b/s/Hz transmission (Fig. 11) is around 5 dB at a BER of 10^{-2}.

For a 6-b/s/Hz transmission and a BER of 10^{-2}, the combined effect degrades the 4×4 SM performance by about 5 dB and the 2×4 SM performance by 3 dB. The effect on V-BLAST's performance is more severe, and a loss in SNR of approximately 8 dB at a BER of 10^{-2} is noticed. For an 8-b/s/Hz transmission at the same BER, the 4×4 and the 8×4 SM systems suffer from 2- and 5-dB losses in SNR, respectively. Again, the effect on V-BLAST is more pronounced, and a loss in SNR of approximately 10 dB is noticed. The high loss in V-BLAST's performance in the presence of all channel imperfections explains why the Alamouti scheme has a better performance than V-BLAST in such channel conditions. At a BER of 10^{-2}, SM outperforms V-BLAST by about 8 dB in both 6- and 8-b/s/Hz transmissions.

In Figs. 10 and 11, both SM schemes show approximately the same BER versus SNR behavior. This is in contrast to previous results, in which SM systems with a low number of transmit antennas performed better than SM systems with a high number of transmit antennas. An explanation is given by noting that the degradation of SM systems, as discussed in the previous paragraph, in the presence of all channel imperfections, increases with an increasing number of transmit antennas. This means that the presence of all channel impairments affects the detection of the transmit antenna number to a greater extent. Therefore, the BER improvement for SM systems with a low number of transmit antennas at a high SNR is considerably less marked than for an ideal channel. For this reason, the SM systems perform almost the same at a high SNR.

C. Coded System With All Channel Imperfections

For coded systems, we consider a convolutional channel encoder, followed by a block interleaver. Each transmitted OFDM frame is independently encoded by the channel encoder and is, then, interleaved by the block interleaver. A nonrecursive rate of 1/2 convolutional encoder, with an overall constraint length of 3, is used. The data that were received after OFDM demodulation are block deinterleaved and are, then, decoded using a hard Viterbi decoder.

The BER performance of coded SM, Alamouti, and V-BLAST with all channel imperfections is depicted in Figs. 12 and 13 for 6- and 8-b/s/Hz transmissions, respectively.

First, a coding gain of approximately 5 dB is evident in both figures, as compared to the previous uncoded results. Second, the SM results show the best performance, and they outperform both Alamouti and V-BLAST. For the case of the 8-b/s/Hz transmission, as shown in Fig. 13, SM outperforms Alamouti by 5 dB and outperforms V-BLAST by 7 dB at a BER of 10^{-3},

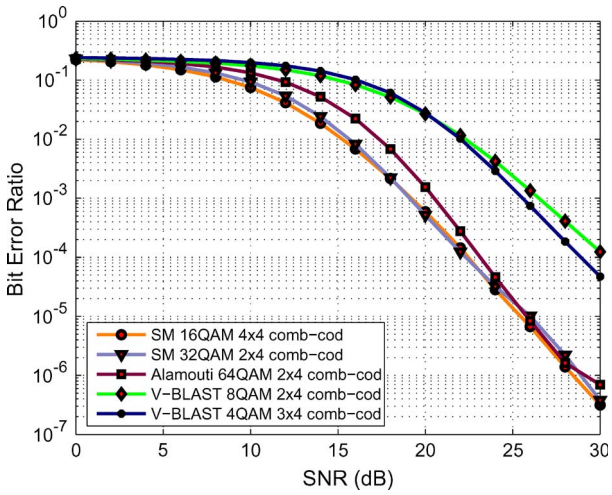

Fig. 12. BER versus SNR for the case of a 6-b/s/Hz transmission (coded combined channel imperfections).

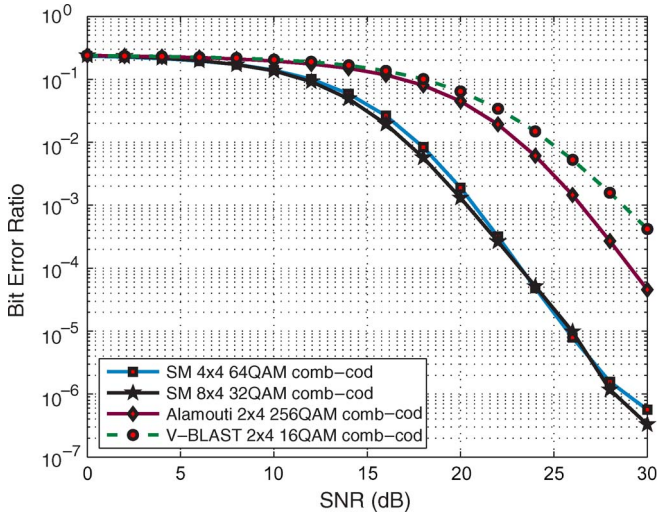

Fig. 13. BER versus SNR for the case of an 8-b/s/Hz transmission (coded combined channel imperfections).

respectively. For the 6-b/s/Hz transmission, SM and Alamouti have almost the same performance at a high SNR, whereas SM outperforms Alamouti by about 1 or 2 dB for SNR < 23 dB. Finally, SM outperforms V-BLAST by about 7 dB in the best case at a BER of 10^{-4}, as shown in Fig. 13.

VI. Receiver Complexity

In this section, we compare the complexity (the number of complex operations) of the V-BLAST, Alamouti, and SM algorithms that were presented in this paper. There are many variants of the original V-BLAST algorithm, some of which, in fact, result in reduced receiver complexity. These algorithms are based on $\mathbf{QR}$ decomposition [46], [47], Gram–Schmitt Orthogonalization, which substitutes the computation of pseudoinverse in finding the weight vectors [48], and the use of a recursive matrix update, as proposed in [49]. However, the reduction in receiver complexity is only significant for a large number of transmit and receive antennas, whereas it is inferior for small numbers. For instance, the proposed scheme in [48] reduces the receiver complexity by 30% for a 4×4 system and by 20% for a 2×4 system. It will be shown in the following that SM yields a greater reduction in receiver complexity than the variants of V-BLAST. In particular, SM has around 90% and 80% reduction in receiver complexity, as compared to MMSE V-BLAST and to V-BLAST-based $\mathbf{QR}$ decomposition, respectively, without sacrificing spectral efficiency. Furthermore, as shown in Section V, SM results in better BER performance for the studied scenarios which do incorporate realistic assumptions regarding the channel. The Alamouti and STCs techniques, on the other hand, are well known to achieve very low receiver complexity. It will be shown that SM achieves complexity that is comparable to those techniques, while superior BER performance is reported in Section V.

Only multiplication and addition of complex numbers are considered as operations. The MMSE criterion requires two matrix multiplications: 1) one inversion and 2) one addition. It is assumed that the matrix transposes are not explicitly computed. The first matrix multiplication requires $N_t^2 N_r$ operations, the matrix addition requires N_t^2 operations, and the matrix inverse needs $4N_t^3$ (using Gaussian elimination) operations [50], [51]. The second matrix multiplication takes N_t^3 operations. Therefore, a total of $(5N_t^3 + N_r N_t^2 + N_t^2)$ complex operations are needed. For V-BLAST, these steps are repeated for $i = 1, \ldots, N_t$. This means that the inverse is computed for a deflated matrix, with decreasing dimensions of $(N_r \times (N_t - \xi)), \xi = 0, \ldots, N_t - 1$. As a result, the total number of complex operations is given by

$$\sum_{i=1}^{N_t} (5i^3 + N_r i^2 + i^2).$$

For V-BLAST with $\mathbf{QR}$ decomposition [52], the computational time is dominated by finding the $\mathbf{QR}$ factorization. The $\mathbf{QR}$ decomposition can be done by directly applying the Householder unitary transformations, which costs $2N_t^2(N_r - (N_t/3))$ complex operations [51]. Filtering the received vector through $\mathbf{Q}^H$ requires N_r^2 operations. For backward and forward sweeps, twice this number of complex operations is needed. Thus, a total of $2(2N_t^2(N_r - (N_t/3)) + N_r^2)$ complex operations are needed.

SM applies MRRC at the receiver. MRRC needs $N_t N_r$ complex multiplications and $N_t(N_r - 1)$ complex additions. Thus, a total of

$$(2N_t N_r - N_t)$$

complex operations are required.

The Alamouti detection process requires N_r^2 complex multiplications and $2(2N_r - 1)$ complex additions for two transmitted symbols. Therefore, a total of $0.5(N_r^2 + 4N_r - 2)$ complex operations are required at the receiver for the detection of one OFDM subchannel.

The required number of complex operations per OFDM subchannel for transmitting six information bits at a time for SM–OFDM, Alamouti–OFDM, and V-BLAST–OFDM are shown in Table III and Fig. 14.

TABLE III
RECEIVER COMPLEXITY COMPARISON FOR A 6-b/s/Hz TRANSMISSION

V-BLAST				SM		Alamouti
MMSE		**QR**		MRRC		ML
2x4 8QAM	3x4 4QAM	2x4 8QAM	3x4 4QAM	4x4 16QAM	2x4 32QAM	2x4 64QAM
110	560	85	140	28	14	15

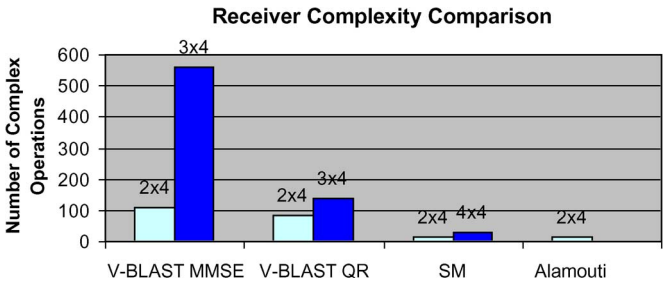

Fig. 14. Receiver complexity comparison for the 6-b/s/Hz transmission that uses MMSE V-BLAST, V-BLAST-based **QR** decomposition, SM, and the Alamouti algorithm.

VII. CONCLUSION

A practical multiple antenna transmission approach, called SM, has been applied to OFDM and has been presented in this paper. The closed-form analytical performance of SM in i.i.d. Rayleigh flat-fading channels has been derived, and analytical and simulation results were shown to closely agree. The SM scheme was shown to be more robust to the presence of Rician fading, SC, and MC, as compared to V-BLAST. In addition, when comparing the performance of SM and Alamouti, SM was shown to have a better or, in the worst case, a similar performance for all the simulated cases. The performance of SM degrades in the presence of a LOS component, whereas the performance of Alamouti improves in such channel conditions. Another limitation of SM is the increase in spectral efficiency by the base-two logarithm of the total number of transmit antennas, as compared to a linear increase for the V-BLAST system.

The obtained gain in the SNR for the same spectral efficiency of SM over V-BLAST at a BER of 10^{-4} varies from 3 dB in ideal channel conditions to 8 dB in the presence of all channel imperfections, along with channel coding. In addition, around 90% of reduction in receiver complexity is achieved. As compared to Alamouti, different performance gains in SNR can be noticed. In the presence of all channel imperfections, along with channel coding, SM gains 1 and 5 dB in SNR over Alamouti for 6- and 8-b/s/Hz transmissions, respectively. Moreover, SM and Alamouti have comparable receiver complexity. An additional significant advantage of SM is the freedom to work with any system configuration, even for the case where there are more transmit antennas than receive antennas.

Future work will concentrate on the investigation of adaptive algorithms to trade off "SM" against signal modulation based on the actual signal-to-interference-plus-noise ratio, as well as new antenna number detection algorithms.

ACKNOWLEDGMENT

The authors would like to thank Prof. McDonough, who was the former vice chair of the Electrical Engineering Program, APL Submarine Technology Department, John Hopkins University, for his very useful comments.

REFERENCES

[1] E. Telatar, "Capacity of multi-antenna Gaussian channels," *Eur. Trans. Telecommun.*, vol. 10, no. 6, pp. 558–595, Nov./Dec. 1999.
[2] G. J. Foschini and M. J. Gans, "On limits of wireless communications in a fading environment when using multiple antennas," in *Wirel. Pers. Commun.*, vol. 1.6. Norwell, MA: Kluwer, 1998, pp. 311–335.
[3] G. J. Foschini, "Layered space-time architecture for wireless communication in a fading environment when using multi-element antennas," *Bell Labs Tech. J.*, vol. 1, no. 2, pp. 41–59, Sep. 1996.
[4] Y. J. Zhang and K. Letaief, "Adaptive resource allocation for multiaccess MIMO/OFDM systems with matched filtering," *IEEE Trans. Commun.*, vol. 53, no. 11, pp. 1810–1816, Nov. 2005.
[5] Y. Li, J. Winters, and N. Sollenberger, "MIMO-OFDM for wireless communications: Signal detection with enhanced channel estimation," *IEEE Trans. Commun.*, vol. 50, no. 9, pp. 1471–1477, Sep. 2002.
[6] IEEE 802.11a, *IEEE Part II: Wireless LAN Medium Access Control (MAC) and Physical Layer (PHY) Specifications: High-Speed Physical Layer in the 5-GHz Band*, 1999. Retrieved Oct. 10, 2006 from [Online]. Available: http://standards.ieee.org/getieee802/802.11.html
[7] IEEE 802.16a, *Local and Metropolitan Area Networks—Part 16: Air Interface for Fixed Broadband Wireless Access Systems*, 2001. Retrieved Oct. 10, 2006 from [Online]. Available: http://standards.ieee.org/catalog/olis/lanman.html
[8] S. Alamouti, "A simple transmit diversity technique for wireless communications," *IEEE J. Sel. Areas Commun.*, vol. 16, no. 8, pp. 1451–1458, Oct. 1998.
[9] V. Tarokh, N. Seshadri, and A. Calderbank, "Space-time codes for high data rate wireless communication: Performance criterion and code construction," *IEEE Trans. Inf. Theory*, vol. 44, no. 2, pp. 744–765, Mar. 1998.
[10] H. El Gamal, "On the robustness of space-time coding," *IEEE Trans. Signal Process.*, vol. 50, no. 10, pp. 2417–2428, Oct. 2002.
[11] M. Godavarti, T. Marzetta, and S. Shamai, "Capacity of a mobile multiple-antenna wireless link with isotropically random Rician fading," *IEEE Trans. Inf. Theory*, vol. 49, no. 12, pp. 3330–3334, Dec. 2003.
[12] P. Viswanath, D. Tse, and V. Anantharam, "Asymptotically optimal water filling in vector multiple-access channels," *IEEE Trans. Inf. Theory*, vol. 47, no. 1, pp. 241–267, Jan. 2001.
[13] G. Raleigh and J. Cioffi, "Spatio-temporal coding for wireless communication," *IEEE Trans. Commun.*, vol. 46, no. 3, pp. 357–366, Mar. 1998.
[14] P. Wolniansky, G. Foschini, G. Golden, and R. Valenzuela, "V-BLAST: An architecture for realizing very high data rates over the rich-scattering wireless channel," in *Proc. URSI ISSSE*, Sep. 29–Oct. 2, 1998, pp. 295–300.
[15] S. Haykin and M. Moher, *Modern Wireless Communications*. Englewood Cliffs, NJ: Prentice-Hall, 2003.
[16] H. Jafarkhani, *Space-Time Coding: Theory and Practice*. Cambridge, U.K.: Cambridge Univ. Press, 2005.
[17] A. Goldsmith, S. Jafar, N. Jindal, and S. Vishwanath, "Capacity limits of MIMO channels," *IEEE J. Sel. Areas Commun.*, vol. 21, no. 5, pp. 684–702, Jun. 2003.
[18] M. Damen, A. Abdi, and M. Kaveh, "On the effect of correlated fading on several space-time coding and detection schemes," in *Proc. IEEE 54th Veh. Technol. Conf.*, Oct. 7–11, 2001, vol. 1, pp. 13–16.
[19] M. Chiani, M. Win, and A. Zanella, "On the capacity of spatially correlated MIMO Rayleigh-fading channels," *IEEE Trans. Inf. Theory*, vol. 49, no. 10, pp. 2363–2371, Oct. 2003.
[20] T. Svantesson and A. Ranheim, "Mutual coupling effects on the capacity of multielement antenna systems," in *Proc. IEEE ICASSP*, May 7–11, 2001, vol. 4, pp. 2485–2488.
[21] S. Ganesan, R. Mesleh, H. Haas, C. W. Ahn, and S. Yun, "On the performance of spatial modulation OFDM," in *Proc. 40th Asilomar Conf. Signals, Syst. Comput.*, Oct. 29–Nov. 1, 2006, pp. 1825–1829.
[22] R. Mesleh, H. Haas, C. W. Ahn, and S. Yun, "Spatial modulation—A new low-complexity spectral efficiency enhancing technique," in *Proc. CHINACOM*, Oct. 25–27, 2006, pp. 1–5.
[23] R. Mesleh, H. Haas, C. W. Ahn, and S. Yun, "Spatial modulation–OFDM," in *Proc. 11th InOWo*, Aug. 30–31, 2006, pp. 288–292.
[24] A. Tonello, "Space-time bit-interleaved coded modulation with an iterative decoding strategy," in *Proc. IEEE 52nd Veh. Technol. Conf.*, Sep. 24–28, 2000, vol. 1, pp. 473–478.

[25] R. Piechocki, P. Fletcher, A. Nix, C. Canagarajah, and J. McGeehan, "Performance evaluation of BLAST-OFDM enhanced hiperlan/2 using simulated and measured channel data," *Electron. Lett.*, vol. 37, no. 18, pp. 1137–1139, Aug. 30, 2001.
[26] K. Lee and D. Williams, "A space-frequency transmitter diversity technique for OFDM systems," in *Proc. IEEE GLOBECOM*, Nov. 27–Dec. 1, 2000, vol. 3, pp. 1473–1477.
[27] BROADCOM Corp., *802.11n: Next-Generation Wireless LAN Technology*, Apr. 2006. White paper, retrieved Aug. 4, 2006. [Online]. Available: http://www.broadcom.com/docs/WLAN/802-11n-WP100-R.pdf
[28] M.-S. Alouini and A. Goldsmith, "A unified approach for calculating error rates of linearly modulated signals over generalized fading channels," *IEEE Trans. Commun.*, vol. 47, no. 9, pp. 1324–1334, Sep. 1999.
[29] J. G. Proakis, *Digital Communications*, 4th ed. New York: McGraw-Hill, 2000.
[30] G. Casella and R. L. Berger, *Statistical Inference*, 2nd ed. ser. Duxbury Advanced. Pacific Grove, CA: Duxbury, 2002.
[31] M. Sellathurai and S. Haykin, "Turbo-BLAST for wireless communications: Theory and experiments," *IEEE Trans. Signal Process.*, vol. 50, no. 10, pp. 2538–2546, Oct. 2002.
[32] M. Pätzold, *Mobile Fading Channels*. Chichester, U.K.: Wiley, 2002.
[33] P. Höher, "A statistical discrete-time model for the WSSUS multipath channel," *IEEE Trans. Veh. Technol.*, vol. 41, no. 4, pp. 461–468, Nov. 1992.
[34] J. Medbo and P. Schramm, *Channel Models for HIPERLAN 2*, 1998. ETSI/BRAN Document No. 3ERIO85B.
[35] A. Paulraj, R. Nabar, and D. Gore, *Introduction to Space-Time Wireless Communications*. Cambridge, U.K.: Cambridge Univ. Press, 2003.
[36] A. Hottinen, O. Tirkkonen, and R. Wichman, *Multi-Antenna Tansceiver Techniques for 3G and Beyond*. Hoboken, NJ: Wiley, 2003.
[37] A. Forenza, D. Love, and R. Heath, Jr., "A low complexity algorithm to simulate the spatial covariance matrix for clustered MIMO channel models," in *Proc. IEEE VTC—Fall*, May 17–19, 2004, vol. 2, pp. 889–893.
[38] H. Özcelik, M. Herdin, W. Weichselberger, J. Wallace, and E. Bonek, "Deficiencies of 'Kronecker' MIMO radio channel model," *Electron. Lett.*, vol. 39, no. 16, pp. 1209–1210, Aug. 2003.
[39] 3GPP, "Spatial Channel Model for Multiple-Input Multiple-Output (MIMO) simulations (Release 6)," *3GPP TR 25.996 V 6.1.0(2003-09)*, 2003. Retrieved Sep. 1, 2006 [Online]. Available: www.3gpp.org/specs/
[40] K. Pedersen, P. Mogensen, and B. Fleury, "A stochastic model of the temporal and azimuthal dispersion seen at the base station in outdoor propagation environments," *IEEE Trans. Veh. Technol.*, vol. 49, no. 2, pp. 437–447, Mar. 2000.
[41] C. A. Balanis, *Antenna Theory Analysis and Design*. New York: Wiley, 1997.
[42] M. Carroll and T. Wysocki, "Fading characteristics for indoor wireless channels at 5-GHz unlicensed bands," in *Proc. IEEE Joint 1st Workshop SympoTIC*, Oct. 26–28, 2003, pp. 102–105.
[43] S. Parker, M. Sandell, and M. Lee, "The performance of space-time codes in office environments," in *Proc. 57th IEEE Semiannual VTC*, Apr. 22–25, 2003, vol. 1, pp. 741–745.
[44] Y. Kim, H. Kang, and K. Kim, "Performance of space-time block codes with QAM under the spatially correlated channels," in *Proc. IEEE 59th VTC—Spring*, May 17–19, 2004, vol. 2, pp. 670–673.
[45] A. Abouda, H. El-Sallabi, and S. Haggman, "Effect of mutual coupling on BER performance of Alamouti scheme," in *Proc. IEEE Antennas Propag. Soc. Int. Symp.*, 2006, pp. 4797–4800.
[46] D. Wubben, R. Bohnke, V. Kuhn, and K.-D. Kammeyer, "MMSE extension of V-BLAST based on sorted QR decomposition," in *Proc. IEEE VTC—Fall*, Oct. 6–9, 2003, vol. 1, pp. 508–512.
[47] K. Kusume, M. Joham, and W. Utschick, "MMSE block decision-feedback equalizer for spatial multiplexing with reduced complexity," in *Proc. IEEE GLOBECOM*, Nov. 29–Dec. 3, 2004, vol. 4, pp. 2540–2544.
[48] W. K. Wai, C.-Y. Tsui, and R. Cheng, "A low-complexity architecture of the V-BLAST system," in *Proc. IEEE WCNC*, Sep. 23–28, 2000, vol. 1, pp. 310–314.
[49] J. Benesty, Y. Huang, and J. Chen, "A fast recursive algorithm for optimum sequential signal detection in a BLAST system," *IEEE Trans. Signal Process.*, vol. 51, no. 7, pp. 1722–1730, Jul. 2003.
[50] N. J. Higham and R. S. Schreiber, "Fast polar decomposition of an arbitrary matrix," *SIAM J. Sci. Stat. Comput.*, vol. 11, no. 4, pp. 648–655, Jul. 1990.
[51] G. H. Golub and C. F. V. Loan, *Matrix Computations*, 3rd ed. Baltimore, MD: Johns Hopkins Univ. Press, 1996.
[52] M. Damen, K. Abed-Meraim, and S. Burykh, "Iterative QR detection for BLAST," *Wirel. Pers. Commun.*, vol. 19, no. 3, pp. 179–191, Dec. 2001.
[53] H. Haas and S. McLaughlin, eds., *Next Generation Mobile Access Technologies: Implementing TDD*. Cambridge, U.K.: Cambridge Univ. Press, Jan. 2008.

Raed Y. Mesleh (S'00–M'08) received the B.Sc. degree in communication engineering from Yarmouk University, Irbid, Jordan, in 2000, the M.Sc. degree in communication technology from Ulm University, Ulm, Germany, in 2004, and the Ph.D. degree in electrical engineering from Jacobs University, Bremen, Germany, in 2007.

From 2000 to 2002, he was with Orange—a mobile operator company in Amman, Jordan—as a Systems Engineer. From 2002 to 2004, he was partly with LogicaCMG as a protocol and testing engineer. Since September 2007, he has been with the School of Electrical Engineering and Computer Science, Jacobs University, where he is currently a Postdoctoral Fellow. His research interests include wireless communications and communication signal processing.

Dr. Mesleh received the Best Student Awards from Yarmouk University and Ulm University.

Harald Haas (S'98–A'00–M'03) received the Ph.D. degree from the University of Edinburgh, Edinburgh, U.K., in 2001.

From 2001 to 2002, he was a Project Manager with Siemens AG (Information and Communication Mobile Networks) for an international research project on new radio access technologies for beyond third-generation (3G) wireless systems. The project involved several Chinese and German universities. In September 2002, he joined the International University Bremen (now Jacobs University), Bremen, Germany, where he is currently an Associate Professor of electrical engineering. In June 2007, he joined the Institute for Digital Communications, University of Edinburgh. He is a coauthor of the *Handbook of Information Security* (Wiley) and *Next Generation Mobile Access Technologies: Implementing TDD* (Cambridge University Press). His work on optical wireless communication was selected for publication in "100 Produkte der Zukunft" by T. W. Hänsch. He is the holder of several patents in wireless communications. His research interests include wireless systems engineering and digital signal processing, in particular, MAC protocols, multiuser access, link adaptation, scheduling, dynamic resource allocation for TDD-based systems, multiple antenna systems, and optical wireless communication.

Dr. Haas received the Best Paper Award at the 10th International Symposium on Personal, Indoor, and Mobile Radio Communications (PIMRC 1999), Osaka/Japan.

Sinan Sinanović received the B.S.E.E. degree (*summa cum laude*) from Lamar University, Beaumont, TX, and the M.S. and Ph.D. degrees in electrical and computer engineering in 2006 from Rice University, Houston, TX.

In 2006, he was with Jacobs University, Bremen, Germany, as a Postdoctoral Fellow. In 2007, he joined the University of Edinburgh, Edinburgh, U.K., where he is currently a Research Fellow with the Institute for Digital Communications. He was with Texas Instruments, Dallas, TX, working on ASIC for the central office modem. While working for Halliburton Energy Services, Houston, he developed an acoustic telemetry receiver. He is the holder of a patent for a directional acoustic telemetry receiver (U.S. patent 7 158 446).

Dr. Sinanović is a member of the Tau Beta Pi and Eta Kappa Nu Electrical Engineering Honor Societies.

Chang Wook Ahn (S'02–M'05) received the B.S. and M.S. degrees in electrical engineering from Korea University, Seoul, Korea, in 1998 and 2000, respectively, and the Ph.D. degree from Gwangju Institute of Science and Technology (GIST), Kwangju, Korea, in 2005.

In 2003, he was a Visiting Scholar with the Illinois Genetic Algorithms Laboratory (IlliGAL), University of Illinois, Urbana-Champaign. From 2005 to 2007, he was a Research Staff Member with the 4G Communication Research Group, Samsung Advanced Institute of Technology. From 2007 to 2008, he was a Research Professor with GIST. Since 2008, he has been with the Department of Computer Engineering, Sungkyunkwan University, Suwon, Korea, as a Faculty Member. His research interests include intelligent wireless networks, machine learning, and evolutionary algorithms.

Sangboh Yun (M'97–S'99–M'02) received the B.S., M.S., and Ph.D. degrees in electrical engineering from Korea University, Seoul, Korea in 1994, 1998, and 2006, respectively.

From 1994 to 2000, he was with Daewoo Telecom, Inc., as a Research Engineer. From 2000 to 2001, he was the Chief Technical Officer with NeoSolution, Inc., where he is also a Cofounder. In 2001, he joined Samsung Advanced Institute of Technology, Kiheung, Korea, as a member of Technical Staff. In 2006, he joined the Telecommunication R&D Center, Samsung Electronics Company, Ltd., Suwon. His research interests include IMT-advanced wireless communication systems, multihop relay, and radio resource management.